Available online at www.sciencedirect.com
SCIENCE DIRECT®
International Journal of Solids and Structures 42 (2005) 2287–2301
INTERNATIONAL JOURNAL OF SOLIDS and STRUCTURES
www.elsevier.com/locate/ijsolstr

Threefold-symmetric Bricard linkages for deployable structures

Yan Chen [a], Zhong You [a], Tibor Tarnai [b,*]

[a] *Department of Engineering Science, University of Oxford, Parks Road, Oxford OX1 3PJ, UK*
[b] *Magdalen College, Oxford OX1 4AU, UK*

Received 5 March 2004; received in revised form 10 September 2004
Available online 2 November 2004

Abstract

A closed-loop overconstrained spatial mechanism composed of six hinge-jointed bars, which has three planes of symmetry in any position, is called a threefold-symmetric Bricard linkage. In this paper a kinematic analysis of these linkages is presented. It is pointed out that for particular parameter values, kinematic bifurcation of the linkages can occur. Features of the kinematic bifurcation are discussed in detail. The applicability of threefold-symmetric Bricard linkages and of their alternative forms to deployable structures is investigated. In addition, by using the theory of kinematic bifurcation, a snap-through phenomenon appearing in a deployable hexagonal ring is explained.

Keywords: Symmetry; Mechanism; State of self-stress; Bricard linkages; Deployable structures; Kinematic bifurcation

1. Introduction

For space technology applications, many deployable structures have been developed that form a single, closed loop (Pellegrino and You, 1993; You and Pellegrino, 1997). Recently Gan and Pellegrino (2003) have suggested spatial mechanical linkages for those purposes. These are composed of four or six bars sequentially connected to each other by simple hinges (“revolute joints”), such that they form a regular planar polygon when fully deployed, and a bundle of bars when fully folded. These closed-loop linkages are in fact overconstrained mechanisms. That means that they should be rigid structures because of their topological

* Corresponding author. Permanent Address: Department of Structural Mechanics, Budapest University of Technology and Economics, Budapest, Műegyetem rkp. 3., H-1521 Hungary. Tel.: +36 1 463 1431; fax: +36 1 463 1099.
E-mail address: tarnai@ep-mech.me.bme.hu (T. Tarnai).

0020-7683/$ - see front matter
doi:10.1016/j.ijsolstr.2004.09.014

properties according to the Kutzbach criterion (Hunt, 1978); and they are mobile only because of their special geometrical properties.

Single, closed-loop overconstrained mechanisms with revolute joints can have two, three, four, five or six links, but in this paper we focus only on six-bar linkages. Among six-bar overconstrained mechanisms with revolute joints, the most remarkable are ''Bricard linkages''. Bricard described three different types of mobile octahedra (Bricard, 1897), and later three additional types of mobile linkages, namely the line-symmetric, the plane-symmetric and the trihedral linkages (Bricard, 1927). Bennett (1911) studied the geometry of the three types of deformable octahedra, and presented the kinematic properties of these mechanisms. But a thorough analysis of all six Bricard linkages was done by Baker (1980), who delineated them by appropriate sets of independent closure equations. The six types of Bricard linkage are the only six-bar, closed-loop mechanisms with revolute joints which are independent of four-bar or five-bar mechanisms. Other six-bar spatial mechanisms with revolute hinges, such as the linkages discovered by Sarrus (1853), Bennett (1905), Goldberg (1943), Waldron (1968), Wohlhart (1991), Mavroidis and Roth (1995), Dietmeier (1995), can be obtained by combining or generalising four-bar or five-bar linkages. Interestingly, Wohlhart (1987) presented a new six-bar linkage, which can be regarded as a generalisation of Bricard's trihedral linkage.

Consider a chain of equal tetrahedra composed of equal isosceles triangles, where each tetrahedron is linked to an adjoining one along an edge, which is the base of a triangle. If the height of the triangles is not smaller than their base, and the number of tetrahedra is six, the ends of the chain can be brought together to form a closed loop. This ring of tetrahedra can turn round with continuous motion like a smoke-ring. This kind of mechanism was invented in Switzerland in 1929 by P. Schatz (see a description of it in Zahaurek (1999) and Schatz (1998)), and independently in the US in 1935 (we could not discover the name of the inventor, but the patent number is given in Ball and Coxeter (1987)). Then it was reinvented by Goldberg (1943) and later by Schattschneider and Walker (1977). According to Ball and Coxeter (1987), the ring of regular tetrahedra was discovered independently by J.M. Andreas and R.M. Stalker, probably earlier than the others; but we have not been able to discover when.

Two main features of the ring of six tetrahedra are: (a) the ring has three planes of symmetry in every position, (b) two edges of every tetrahedron, about which the adjacent tetrahedra rotate, are perpendicular to each other. The ring of tetrahedra in fact is a special case of both the plane-symmetric and the trihedral Bricard linkages. If perpendicularity of the adjacent revolute joints is dropped, but the three planes of symmetry are preserved, the linkages are still able to move. These six-bar, closed-loop spatial mechanisms with revolute joints, which have three planes of symmetry in any position, are called *threefold-symmetric Bricard linkages*. To our knowledge, the properties and practical applicability of these linkages have not yet been studied, apart from a paper by Gan and Pellegrino (2003).

The aim of this paper is to discover the characteristics of threefold-symmetric Bricard linkages. It will be shown that, for certain geometrical parameters, kinematic bifurcation can occur. Kinematic bifurcation of these linkages is a fascinating phenomenon, because these linkages are overconstrained mechanisms which can have a configuration-dependent state of self-stress. Bifurcation can be analysed in terms of small imperfections (Tarnai, 2001; Lengyel, 2002; Lengyel and You, 2004). Here, however, geometrical imperfections cannot be arbitrary, but must be special ones for which the movability of the linkage is preserved. In particular, for arbitrary geometrical imperfections, the mechanism would become a rigid structure, and the state of self-stress would disappear.

If a link other than that perpendicular to both axes of two adjacent hinges is used physically to connect the two hinges, then an alternative form of the linkage is obtained. We shall investigate alternative forms of threefold-symmetric Bricard linkages in order to find good solutions to deployable structures of closed-loop form. Two physical models were made on the basis of the same alternative form, and it was found that one of them was able to move from the deployed configuration to the folded one, while the other was blocked at a certain intermediate stage; and it was able to continue its motion only if it was

forced to do so. Using the theory of kinematic bifurcation, we shall give an insight into this striking phenomenon.

The scheme of the present paper is as follows. A technical description of the analysis of motion of threefold-symmetric Bricard linkages is given in Section 2, where their general properties are also presented. Section 3 then studies the kinematic bifurcation of these linkages for particular parameter values. Section 4 discusses an application of these linkages as deployable structures. Finally, conclusions are drawn in Section 5.

2. General properties of the linkage

Denavit and Hartenberg (1955) set forth a standard approach to the analysis of spatial linkages, where geometric conditions are taken into account. They pointed out that the necessary and sufficient condition that a loop in a linkage is closed is that the product of the transfer matrices equals the identity matrix, i.e.,

$$[T_{n1}]\cdots[T_{34}][T_{23}][T_{12}] = [I] \tag{1}$$

(this is known as *loop closure equation*). In (1), $[T_{i(i+1)}]$ is the transfer matrix that, in a homogeneous form, transforms the coordinate system X_i, Y_i, Z_i attached to link $(i-1)i$, i.e., the link connecting joints $i-1$ and i, into the coordinate system X_{i+1}, Y_{i+1}, Z_{i+1} attached to link $i(i+1)$, i.e., the link connecting joints i and $i+1$, see Fig. 1(a),

$$\left[T_{i(i+1)}\right] = \begin{bmatrix} 1 & 0 & 0 & 0 \\ -a_{i(i+1)} & C\theta_i & S\theta_i & 0 \\ -R_i S\alpha_{i(i+1)} & -C\alpha_{i(i+1)} S\theta_i & C\alpha_{i(i+1)} C\theta_i & S\alpha_{i(i+1)} \\ -R_i C\alpha_{i(i+1)} & S\alpha_{i(i+1)} S\theta_i & -S\alpha_{i(i+1)} C\theta_i & C\alpha_{i(i+1)} \end{bmatrix}. \tag{2}$$

Here, right-handed Cartesian coordinate systems and "right-hand screw" sign convention for rotations are applied, and the following notation is used: $a_{i(i+1)}$ is the length of link $i(i+1)$, i.e., the distance between axes Z_i and Z_{i+1} of joints i and $i+1$; $\alpha_{i(i+1)}$ is the twist angle between the axes of joints i and $i+1$, i.e., angle of rotation about X_{i+1} that rotates $//Z_i$ to Z_{i+1}; R_i is the offset along joint i, i.e., the distance from link $(i-1)i$ to link $i(i+1)$ considered positive in the direction of Z_i; θ_i is the rotation angle about axis of joint

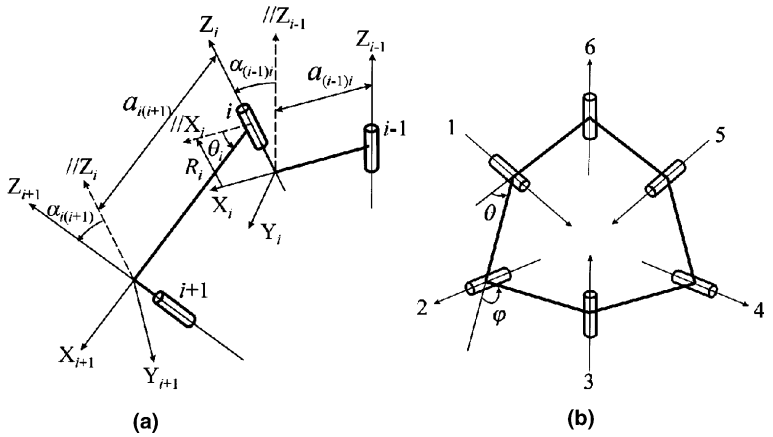

Fig. 1. (a) Coordinate systems for two links connected by a revolute joint; (b) the threefold-symmetric overconstrained mechanism (see (5a) and (5b)).

i, i.e., the angle of rotation about Z_i that rotates $//X_i$ to X_{i+1}. $//X_i$ and $//Z_i$ are axes parallel to X_i and Z_i, respectively. In the case of revolute joints, parameters $a_{i(i+1)}$, $\alpha_{i(i+1)}$, R_i are called *geometric* (*or structural*) *parameters*, and θ_i is called a *revolute* (*or motion*) *variable*. S and C denote sine and cosine. Note that the transfer matrix, transforming the coordinate system attached to link $i(i+1)$ to the coordinate system attached to link $(i-1)i$, is the inverse of $[T_{i(i+1)}]$, i.e.,

$$\left[T_{(i+1)i}\right] = \left[T_{i(i+1)}\right]^{-1} = \begin{bmatrix} 1 & 0 & 0 & 0 \\ a_{i(i+1)}C\theta_i & C\theta_i & -C\alpha_{i(i+1)}S\theta_i & S\alpha_{i(i+1)}S\theta_i \\ a_{i(i+1)}S\theta_i & S\theta_i & C\alpha_{i(i+1)}C\theta_i & -S\alpha_{i(i+1)}C\theta_i \\ R_i & 0 & -S\alpha_{i(i+1)} & C\alpha_{i(i+1)} \end{bmatrix}. \tag{3}$$

Consider a plane-symmetric Bricard linkage with geometric parameters satisfying the following conditions:

$$a_{12} = a_{23} = a_{34} = a_{45} = a_{56} = a_{61} = l, \tag{4a}$$

$$\alpha_{12} = \alpha_{34} = \alpha_{56} = \alpha, \alpha_{23} = \alpha_{45} = \alpha_{61} = 360^\circ - \alpha, \tag{4b}$$

$$R_i = 0 (i = 1, 2, \ldots, 6), \tag{4c}$$

where angles in (4b) are measured in degrees. The linkage thereby obtained has threefold rotational symmetry and also three planes of symmetry. The point group symmetry of such an object is denoted by C_{3v}. A linkage satisfying the special geometric conditions (4a)–(4c) is a *threefold-symmetric Bricard linkage*. The configuration of this linkage is shown in Fig. 1(b). It is easy to see that threefold-symmetric Bricard linkages form a subset of the set of plane-symmetric Bricard linkages. If, as a further specialisation, 90° is selected as the angle α, then relationships (4a)–(4c) satisfy the geometrical conditions of trihedral Bricard linkages (Baker, 1980). Therefore, in this case, a threefold-symmetric Bricard linkage is also a trihedral Bricard linkage.

Next we shall investigate the mobility of a threefold-symmetric Bricard linkage and show that it has a single degree of freedom. Mobility itself, in fact, is not in question because the plane-symmetric property guarantees it; but the number of degrees of freedom is. It is not known whether the number of degrees of freedom increases with an increase in the degree of symmetry. Because of threefold symmetry, the six revolute variables must satisfy the following conditions:

$$\theta_1 = \theta_3 = \theta_5 = \theta, \tag{5a}$$

$$\theta_2 = \theta_4 = \theta_6 = \varphi. \tag{5b}$$

Since we have a six-link, single-loop chain ($n = 6$), the closure condition (1) takes the form

$$[T_{61}][T_{56}][T_{45}][T_{34}][T_{23}][T_{12}] = [I] \tag{6}$$

or

$$[T_{34}][T_{23}][T_{12}] = [T_{54}][T_{65}][T_{16}]. \tag{7}$$

Substituting the geometric parameters (4) and the revolute variables (5) into (7), the closure equation of this threefold-symmetric linkage is obtained:

$$\cos^2\alpha + \sin^2\alpha(\cos\theta + \cos\varphi) + (1 + \cos^2\alpha)\cos\theta\cos\varphi - 2\cos\alpha\sin\theta\sin\varphi = 0. \tag{8}$$

For any given α ($0^\circ \leqslant \alpha \leqslant 180^\circ$), (8) represents the input–output equation. It is apparent that (8) is symmetric in θ and φ (for if these variables are exchanged in (8), Eq. (8) does not change). Therefore, any of θ and φ can be chosen to be the input and the other called the output. Fig. 2(a) shows the input–output

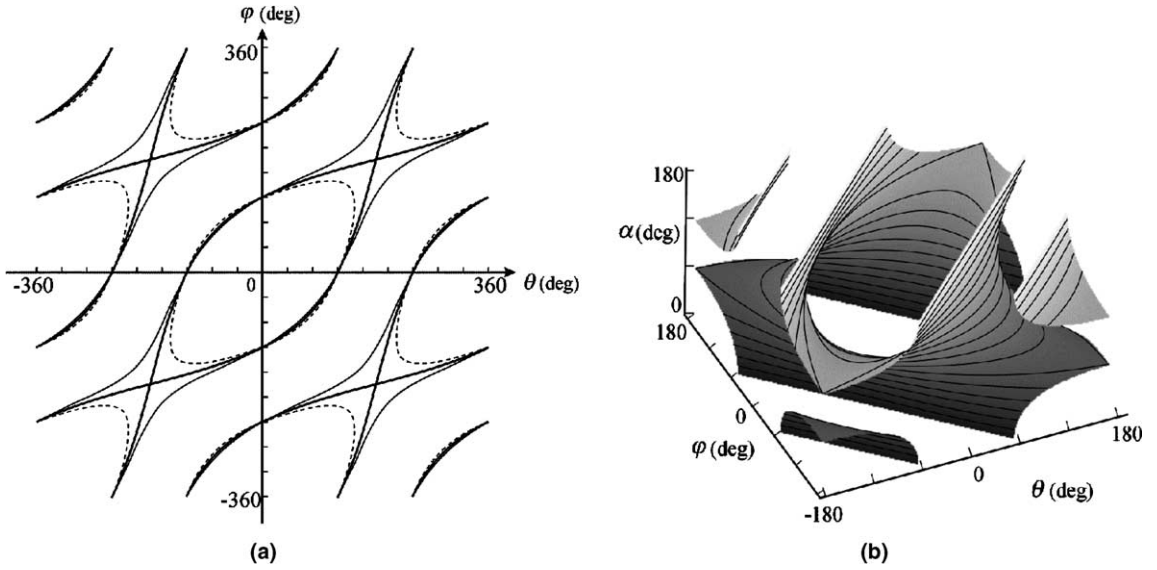

Fig. 2. (a) θ versus φ for the threefold-symmetric linkage for $\alpha = 115°$ (thin dashed line), 120° (thick solid line), 125° (thin solid line); (b) θ versus φ as a function of α for the threefold-symmetric linkage for $0 \leqslant \alpha \leqslant 180^0$ in a period. The α-contours are spaced at 10° intervals.

curve determined by (8). Note that it is periodic. The period for both θ and φ is 360°. An input–output curve is also called a *compatibility path*, mainly in a bifurcation context (Tarnai, 1984; Lengyel and You, 2003).

A number of distinctive features of the threefold-symmetric Bricard linkage with any twist α can be established from Fig. 2. Firstly, it appears that only one of the six revolute variables can be free. Thus, this threefold-symmetric linkage has one degree of finite mobility. Secondly, the linkage with twist α behaves in the same way as one whose twist is $180°-\alpha$. Thirdly, all compatibility paths in the (θ, φ) Cartesian coordinate system pass through the points (0°, −120°), (0°, 120°), (−120°, 0°), and (120°, 0°), regardless the value of α. This means that all of the threefold-symmetric Bricard linkages can be flattened to form a planar equilateral triangle with side length $2l$. Additionally, it has been found by experiment that, for $0° \leqslant \alpha < 60°$ or $120° < \alpha \leqslant 180°$, the movement of linkages is not continuous. Thus, the linkage is physically blocked in the positions where all links cross at the centre when either θ or φ reaches 180° or −180°. When $60° \leqslant \alpha \leqslant 120°$, the linkage keeps moving continuously; each compatibility path forms a closed loop, as in Fig. 2(a) for $\alpha = 115°$.

Consider now the compatibility paths in Fig. 2 for $\alpha = 60°$ or 120°. Here, both θ and φ reach 180° or −180° simultaneously which corresponds to the most compact folding. The physical model shown in Fig. 3(a) demonstrates this feature. When $\theta = 0°$, $\varphi = \pm 120°$, or vice versa, the linkage forms a plane equilateral triangle as mentioned before, in the configuration of maximum expansion (Fig. 3c).

3. Bifurcation of the compatibility path

Motion experiments with physical models for $\alpha = 120°$ show an unusual phenomenon, when the six bars reach the completely folded configuration (Fig. 3a). In a "uniform" motion of the linkage, the lower and the top joints arrive at the fully-folded stage with small and great speed, respectively; but when they start to

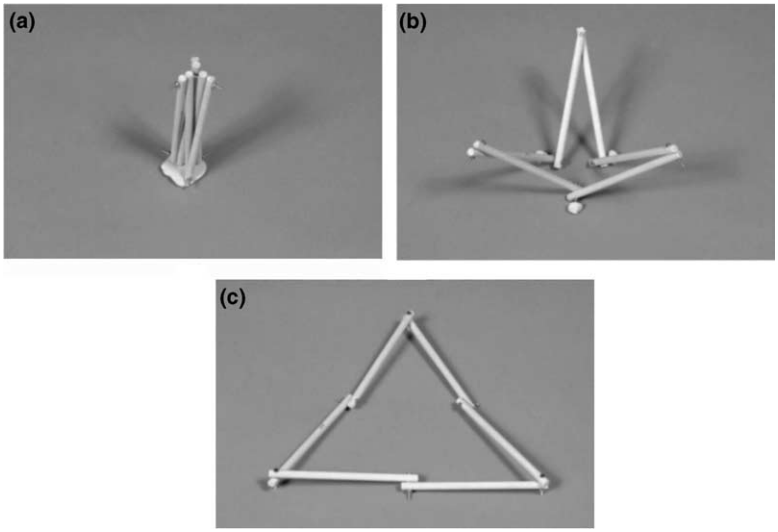

Fig. 3. A model of a threefold-symmetric Bricard linkage with $\alpha = 120°$. (a) The compact folded configuration; (b) the configuration during the process of deployment; (c) the maximum expanded configuration.

move backwards, the lower joints move with great speed and the upper joints with small speed. That is, the velocities of the upper and lower joints are exchanged, and the direction of their motion is inverted. The whole motion seems to be continuous, but the velocity of the joints changes dramatically at the completely folded position, which occurs when both θ and φ are close to 180°. This phenomenon suggests that the fully-folded position should be of particular interest for motion.

Fig. 2 shows that, when $\alpha = 60°$ or 120°, two compatibility paths cross each other at points (−180°, 180°) and (180°, −180°) or (180°, 180°) and (−180°, −180°). This raises the possibility of having a kinematic bifurcation at these four points.

Because of similarity, we need only consider the threefold-symmetric Bricard linkage with $\alpha = 120°$ at point (180°, 180°). The compatibility paths of this linkage in the range $0 \leqslant \theta \leqslant 360°$, $0 \leqslant \varphi \leqslant 360°$ are reproduced in Fig. 4(a). For a small imperfection ε in twist α, the compatibility paths will alter slightly (Fig. 4a). If α is considered as a variable, and the compatibility condition (8) is plotted in 3D, see Fig. 4(b), the surface of compatibility will have a saddle point at $(\theta, \varphi, \alpha) = (180°, 180°, 120°)$. We shall now prove that this is a point of bifurcation.

A characteristic of the bifurcation of compatibility paths is that, at the point of bifurcation, the number of instantaneous (infinitesimal) degrees of freedom increases. In structural terms it means that the degree of kinematic indeterminacy increases (Tarnai, 2001; Lengyel, 2002). For an assembly, however, an increase in the degree of kinematic indeterminacy is coupled to a simultaneous increase in the degree of static indeterminacy (Calladine, 1978; Calladine and Pellegrino, 1991). Therefore, a kinematic bifurcation of a mechanism can be detected by examining the number of independent states of self-stress of the mechanism. Normally, a closed-loop spatial linkage composed of seven bars with revolute joints forms a mechanism with a single degree of mobility. A related linkage with six bars is in general a rigid structure. The threefold-symmetric Bricard linkage as a six-bar mechanism with revolute joints is overconstrained. It has a single degree of mobility; therefore, it must have one state of self-stress in general. By considering the equilibrium of internal forces of the linkage, the existence of a state of self-stress can be shown. Moreover, we can demonstrate that the number of independent states of self-stress becomes two at the point (180°, 180°).

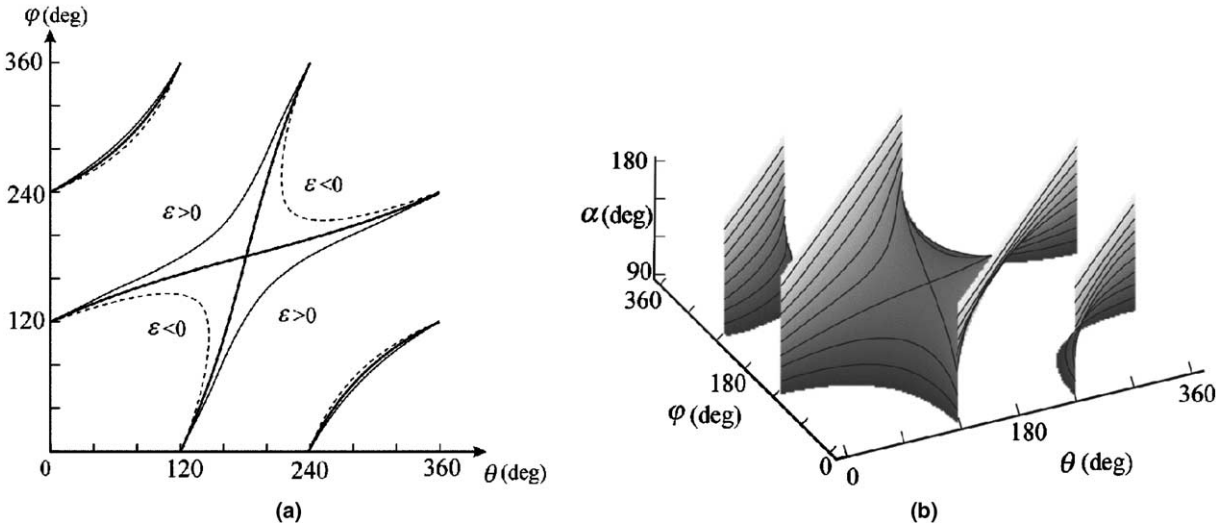

Fig. 4. (a) The compatibility paths of the threefold-symmetric linkage in the range $0 \leqslant \theta \leqslant 360°$, $0 \leqslant \varphi \leqslant 360°$ when $\alpha = 120°$ and $\alpha = 120° \pm \varepsilon$; (b) the compatibility paths of the threefold-symmetric linkage in the range $0 \leqslant \theta \leqslant 360°$, $0 \leqslant \varphi \leqslant 360°$ when $90° \leqslant \alpha \leqslant 180°$. The α-contours are spaced at 10° intervals.

Because of threefold symmetry, all odd-numbered joints with the adjacent two links are geometrically congruent; and the same is separately true for the even-numbered joints. At each joint, two links meet, and there is no external load; so the forces at the ends of the two adjacent links should equilibrate each other. Additionally, the forces at the two ends of each link should be in equilibrium. In this way, all odd-numbered joints are also statically congruent, and separately, the same is true for the even-numbered joints. Therefore, it is sufficient to analyse the equilibrium of two consecutive joints (odd and even).

Consider the threefold-symmetric linkage with link length l. For the typical links 12 and 23, the internal forces and moments at each end are shown in Fig. 5(a). Forces and moments acting at joints 2 and 3, where links 12, 23 and 23, 34 meet, respectively, are shown in Fig. 5(b). Forces and moments are denoted by N and M, respectively, with respective subscripts, and defined in local coordinate systems fitted to both the link and the joint axes. For example, at the end 2 of link 12, forces and moments are defined in the local coordinate system x_{21}, y_{21}, z_{21} in which z_{21} is along the link while y_{21} is along the axis of joint 2. At the end 1, z_{12} is along the link while y_{12} is along the axis of joint 1. Similarly, we can define forces and moments for link 23. Because of symmetry, the local forces and moments in link 34 should be the same as those in link 12.

Writing the equilibrium equations for links 12, 23 and for joints 2, 3 results in a set of homogeneous linear equations with a square coefficient matrix, called the equilibrium matrix, whose rank deficiency is 1. That means that the linkage can have one state of self-stress (Calladine, 1978). (A detailed derivation is given in the Appendix A.) If $\theta = 180°$ and consequently $\varphi = 180°$ when $\alpha = 120°$, then the rank deficiency of the equilibrium matrix is 2; that is the linkage has two states of self-stress. Indeed, we find that

$$Nz_{21} = -Nz_{23}, Nz_{12} = Nz_{23}, Nz_{32} = -Nz_{23}, \tag{9a}$$

$$Mz_{21} = -Mz_{23}, Mz_{12} = Mz_{23}, Mz_{32} = -Mz_{23}, \tag{9b}$$

while all other forces and moments are equal to zero. Thus, all internal forces can be expressed in terms of two parameters: Nz_{23} and Mz_{23}, for instance. In this position, the six links theoretically coincide, and in the consecutive links, there are equal axial forces and equal torques both with alternating sign. Because the degree of static indeterminacy changes from 1 to 2, point (180°, 180°) is a point of kinematic bifurcation.

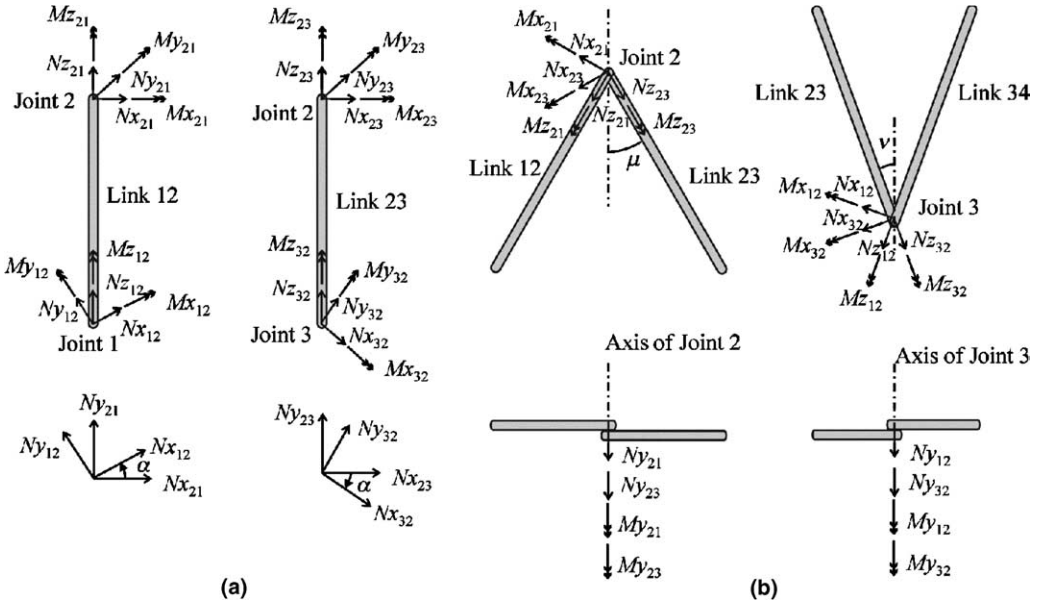

Fig. 5. Equilibrium of a threefold-symmetric Bricard linkage. (a) Forces in links 12 and 23; (b) forces at joints 2 and 3.

The static argument above gives indirect evidence that the kinematic indeterminacy increases by 1 at $\theta = \varphi = 180°$. This result can be obtained also by means of a direct kinematic basis. The physical model shows that, at $\theta = \varphi = 180°$, the degree of infinitesimal mobility increases by 1, because in this configuration, the axes of the three joints at the top are coplanar and intersect at a single point, and so do the axes of the other three joints at the bottom, see Fig. 3(a). This leads to two degrees of infinitesimal mobility (Phillips, 1990). Although bifurcation exists in this configuration, it does not cause any problem in the deployment and folding of the linkage, because the links would have to penetrate each other in order to reach the bifurcated position, which is physically impossible. The movement of the linkage at $\theta = \varphi = 180°$ effectively changes from one path to another, so that the values of θ and φ increase on one path and decrease on the other. In such a situation, one of the two infinitesimal mobilities becomes finite while the other disappears.

4. Deployable structures

Although the original threefold-symmetric Bricard linkage has been shown to produce a compact folded configuration, it is hard to realise it in practice. This is because the angles between six pairs of connected bars cannot become zero simultaneously without a complex design. Hence, it is important to investigate alternative forms of threefold-symmetric Bricard linkages.

One of these alternative forms was found by Gan and Pellegrino (2003). There, the axes of the revolute joints are extended and the joints are connected with bars that are not perpendicular to the joint axes: see Fig. 6, where the dashed lines represent the links of the original linkage and the solid lines represent the bars in the alternative form.

For simplicity, let us assume that the same symmetry is retained in the alternative form. Denote the link length and twist angles of the original threefold-symmetric Bricard linkage in Fig. 6 by l and α (or $360°-\alpha$), respectively. We have

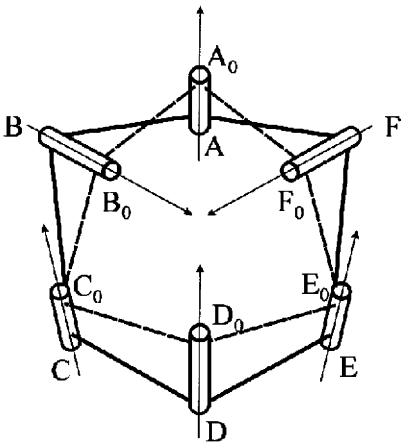

Fig. 6. An alternative form of the threefold-symmetric Bricard linkage.

$$\overline{A_0A} = \overline{C_0C} = \overline{E_0E} = c,$$

$$\overline{B_0B} = \overline{D_0D} = \overline{F_0F} = d.$$

So, all bars of the alternative form have the same length, L, given by

$$\overline{AB} = \overline{BC} = \overline{CD} = \overline{DE} = \overline{EF} = \overline{FA} = L = \sqrt{l^2 + c^2 + d^2 - 2cd\cos\alpha}. \tag{10}$$

For each given set of c and d, an alternative form for the threefold-symmetric Bricard linkage can be obtained. The most compact folding can be achieved if the points A, C and E coincide and simultaneously so do the points B, D and F. This means that physically the linkage becomes a bundle whose length is L. In this fully-folded configuration denote θ and φ by θ_f and φ_f, respectively. On the other hand, when the linkage is fully expanded, points A, B, C, D, E, and F are all in the same plane, i.e., the linkage is completely flattened to form an equilateral hexagon. In this configuration denote θ and φ by θ_d and φ_d, respectively. Several alternative forms with these properties can be obtained.

On the basis of the linkage found by Gan and Pellegrino (2003), we have made an alternative form of a threefold-symmetric Bricard linkage with different parameters. The geometric parameters of the original threefold-symmetric Bricard linkage and its alternative form are

$$\alpha = 180^\circ - \arctan 2, \tag{11a}$$

$$\theta_f = -120^\circ, \quad \varphi_f = -\arctan\frac{\sqrt{15}}{7}, \tag{11b}$$

$$\theta_d = 120^\circ, \quad \varphi_d = 0^\circ, \tag{11c}$$

$$L = \frac{2}{3}\sqrt{3}\cdot l, \quad c = \frac{\sqrt{3}}{6}\cdot l, \quad d = \frac{\sqrt{15}}{6}\cdot l. \tag{11d}$$

The compatibility path of this linkage (which of course is the same for both the original and the alternative form) is shown in Fig. 7. The fully-expanded position, where the linkage is flat, corresponds to point R on the compatibility path, while the completely folded position corresponds to point S. We have made two different physical realisations of this alternative-form linkage. The first was proposed by Pellegrino (private communication): for convenience, let us call it *linkage I*—and the other *linkage II*.

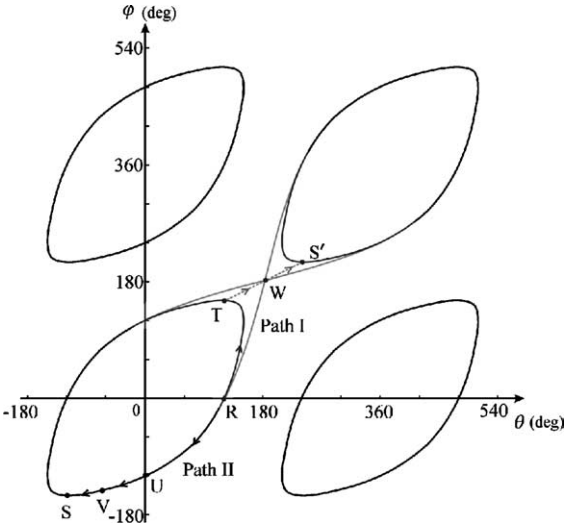

Fig. 7. The compatibility path of the threefold-symmetric linkage with twist $\alpha = 180° - \arctan 2$. *Path I* from R to S' and *path II* from R to S corresponds to the motion of *linkage I* and *linkage II*, respectively.

In the fully-expanded position, where the linkage has a regular hexagonal form, the axis of every second joint is perpendicular to the plane of the hexagon. If equal bars of finite cross-section are used in the physical model, we have *linkage I* or *linkage II*, depending on whether these perpendicular joints are on the internal side (Fig. 8a) or on the external side (Fig. 9a) of the hexagonal ring. These two linkages show an interesting difference in their properties. Although both are based on the *same* alternative form of the *same* threefold-symmetric Bricard linkage, during the folding process, the motion of one of them is blocked but that of the other is not.

For *linkage I*, the folding process can be traced along the compatibility path from R to S via T (Fig. 7). However, the movement of the linkage is found to be physically blocked at point T, because the ends of bars hit each other. If the model is made from solid metal bars and metal hinges, then it is fairly rigid and allows almost no deformation at this stage. Hence, the folding terminates at point T.

Pellegrino (private communication) has also observed that the linkage did fold up if it is made with weak hinges. While folding, a force has to be applied to the linkage to enable the joints to go through some slight elastic deformation. This can be demonstrated by means of the model shown in Fig. 8, which is made of card. When it is folded from the configuration in Fig. 8(a) to that in Fig. 8(b), a force has to be applied to make the model move to the position in Fig. 8(c) and then on to the bundle-form in Fig. 8(d).

A close examination of the compatibility path in Fig. 7 reveals that, in the card model, the folding process corresponds to a movement along *path I* from R to S', instead of S, due to the fact that the compatibility path is periodic and $\theta_{S'} = \theta_S + 360°$, $\varphi_{S'} = \varphi_S + 360°$. The reason why this happens is that $\alpha = 180° - \arctan 2 = 116.57°$, is sufficiently close to 120°. As discussed in Section 3, $\theta = \varphi = 180°$ is a point of kinematic bifurcation for the threefold-symmetric linkage with twist $\alpha = 120°$. Hence, when a force is applied to the linkage with $\alpha = 116.57°$, an imperfection is introduced in the twist of the linkage which changes to 120°. The folding process thus reaches the bifurcation point W. When the force is released, the twist of linkage comes back to $\alpha = 116.57°$. Accordingly, the moving point (θ, φ) reaches point S' (where the physical configuration of the linkage is the same as it would be at S). This is a snap-through phenomenon, where compatibility of the geometrically perfect linkage is temporarily lost, and small angular gaps appear at the hinges.

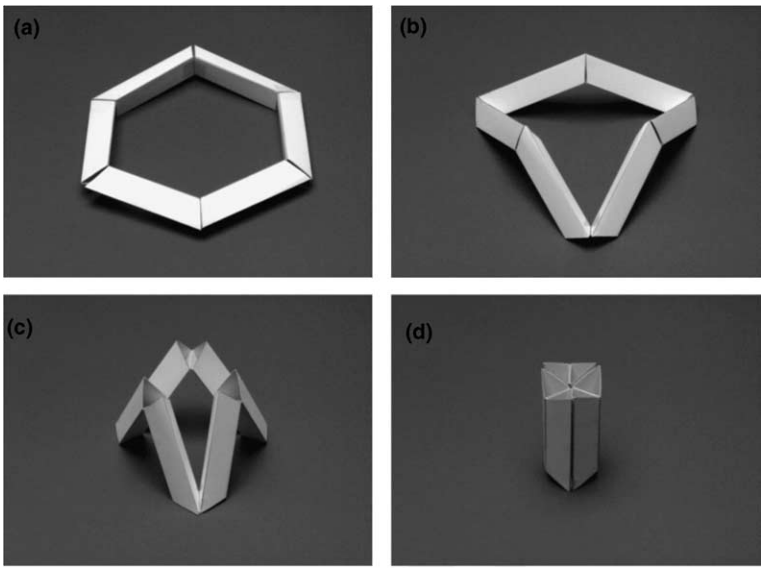

Fig. 8. Card model of *linkage I*. (a) Deployed configuration at point R; (b) configuration at the blocked point T; (c) configuration at the bifurcation point W; (d) fully-folded configuration at point S'. Points R, T, W, S' are shown in Fig. 7.

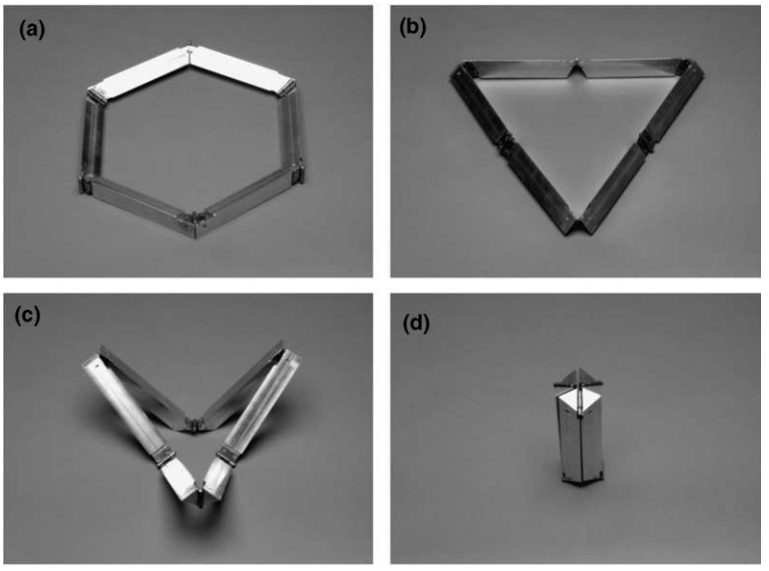

Fig. 9. Metal model of *linkage II*. (a) Deployed configuration at point R; (b) a particular configuration at point U; (c) configuration at point V; (d) fully-folded configuration at point S. Points R, U, V, S are shown in Fig. 7.

Linkage II behaves differently. During the folding process, the actual point (θ, φ) on the compatibility path moves from point R to point S via U and V (*path II* in Fig. 7). There is no blockage during folding, and the linkage can be folded up completely, as shown in Fig. 9. So this model could have been made of cardboard.

5. Conclusions

This paper has analysed the kinematic properties of a group of single, closed-loop, six-bar, spatial linkages derived from the plane-symmetric Bricard linkages. These threefold-symmetric mechanisms are overconstrained, with a single degree of mobility and a single configuration-dependent state of self-stress.

Experiments with physical models and a parametric study of the compatibility paths have led to the discovery of a kinematic bifurcation, that has been proved by the change in number of states of self-stress. Alternative forms of the threefold-symmetric linkages and their applications as deployable structures have also been discussed. These six-bar structures have a deployed configuration as a hexagon and a folded configuration as a bundle. Our understanding of the kinematic bifurcation has helped us to explain a temporary physical incompatibility during the deployment of one of the structures.

The analysis presented in this paper has given a deeper insight into the kinematic behaviour of threefold-symmetric overconstrained mechanisms and their applications in deployable structures. The deployable structures shown in Section 4 are simple examples of practical applications. Further applications are also possible. New deployable structures can be obtained, for instance, by using threefold-symmetric linkages as building-blocks in large lattice-like, multiply overconstrained mechanisms (Chen, 2003). This possibility can open up a new field in the design of deployable structures.

Acknowledgments

Research reported here was partially supported by the European Science Exchange Programme of the Royal Society (HA/ESEP/JP). Support of OTKA grants no. T031931 and T046846 is also acknowledged and appreciated. YC thanks University of Oxford for the graduate scholarship. TT thanks the President and Fellows of Magdalen College, Oxford for their hospitality. The authors are grateful to Professors J.E. Baker and S. Pellegrino for advice, and to Professor C.R. Calladine for comments on an earlier version of the manuscript.

Appendix A

The equilibrium equations for link 12 can be written as

$$Nx_{21} + Nx_{12}\cos\alpha - Ny_{12}\sin\alpha = 0, \tag{A.1a}$$

$$Ny_{21} + Nx_{12}\sin\alpha + Ny_{12}\cos\alpha = 0, \tag{A.1b}$$

$$Nz_{21} + Nz_{12} = 0, \tag{A.1c}$$

$$Mx_{21} + Mx_{12}\cos\alpha - My_{12}\sin\alpha - Ny_{21}\cdot l = 0, \tag{A.1d}$$

$$My_{21} + Mx_{12}\sin\alpha + My_{12}\cos\alpha + Nx_{21}\cdot l = 0, \tag{A.1e}$$

$$Mz_{21} + Mz_{12} = 0. \tag{A.1f}$$

The equilibrium equations for link 23 are:

$$Nx_{32} + Nx_{23}\cos\alpha - Ny_{23}\sin\alpha = 0, \tag{A.2a}$$

$$Ny_{32} + Nx_{23}\sin\alpha + Ny_{23}\cos\alpha = 0, \tag{A.2b}$$

$$Nz_{23} + Nz_{32} = 0, \tag{A.2c}$$

$$Mx_{32} + Mx_{23}\cos\alpha - My_{23}\sin\alpha + Ny_{32}\cdot l = 0, \tag{A.2d}$$

$$My_{32} + Mx_{23}\sin\alpha + My_{23}\cos\alpha - Nx_{32}\cdot l = 0, \tag{A.2e}$$

$$Mz_{23} + Mz_{32} = 0. \tag{A.2f}$$

Links 12 and 23 are connected at joint 2 whose axis is in the same direction as Ny_{21} and Ny_{23}, see Fig. 5(b). The equilibrium equations of joint 2 are:

$$-Nx_{21}\cos\mu - Nx_{23}\cos\mu - Nz_{21}\sin\mu + Nz_{23}\sin\mu = 0, \tag{A.3a}$$

$$-Ny_{21} - Ny_{23} = 0, \tag{A.3b}$$

$$Nx_{21}\sin\mu - Nx_{23}\sin\mu - Nz_{21}\cos\mu - Nz_{23}\cos\mu = 0, \tag{A.3c}$$

$$-Mx_{21}\cos\mu - Mx_{23}\cos\mu - Mz_{21}\sin\mu + Mz_{23}\sin\mu = 0, \tag{A.3d}$$

$$-My_{21} - My_{23} = 0, \tag{A.3e}$$

$$Mx_{21}\sin\mu - Mx_{23}\sin\mu - Mz_{21}\cos\mu - Mz_{23}\cos\mu = 0, \tag{A.3f}$$

where

$$\mu = (180^\circ - \varphi)/2, \tag{A.4}$$

which is the half of the angle between links 12 and 23.

Links 23 and 34 are connected at joint 3 whose axis is in the same direction as Ny_{32} and Ny_{34} which is shown as Ny_{12} in Fig. 5(b), because the forces in link 34 are the same as that in link 12. The equilibrium equations of joint 3 are:

$$-Nx_{12}\cos\nu - Nx_{32}\cos\nu - Nz_{12}\sin\nu + Nz_{32}\sin\nu = 0, \tag{A.5a}$$

$$-Ny_{12} - Ny_{32} = 0, \tag{A.5b}$$

$$Nx_{12}\sin\nu - Nx_{32}\sin\nu - Nz_{12}\cos\nu - Nz_{32}\cos\nu = 0, \tag{A.5c}$$

$$-Mx_{12}\cos\nu - Mx_{32}\cos\nu - Mz_{12}\sin\nu + Mz_{32}\sin\nu = 0, \tag{A.5d}$$

$$-My_{12} - My_{32} = 0, \tag{A.5e}$$

$$Mx_{12}\sin\nu - Mx_{32}\sin\nu - Mz_{12}\cos\nu - Mz_{32}\cos\nu = 0, \tag{A.5f}$$

where

$$\nu = (180^\circ - \theta)/2, \tag{A.6}$$

which is the half of the angle between links 23 and 34. Because a revolute joint cannot carry moment in its axis direction, we have

$$My_{21} = My_{23} = 0, \tag{A.7a}$$

$$My_{12} = My_{32} = 0. \tag{A.7b}$$

By substituting (A.7) into (A.1)–(A.3) and (A.5), we obtain

$$Nx_{21} - Nz_{23} \cdot \tan\mu = 0, \qquad Ny_{21} - Nz_{23} \cdot \frac{\tan v - \tan\mu\cos\alpha}{\sin\alpha} = 0, \qquad Nz_{21} + Nz_{23} = 0, \qquad \text{(A.8a, b, c)}$$

$$Mx_{21} - Nz_{23} \cdot \frac{\tan v}{\sin\alpha} \cdot l = 0, \qquad My_{21} = 0, \qquad Mz_{21} - Nz_{23} \cdot \frac{\tan\mu\tan v}{\sin\alpha} \cdot l = 0, \qquad \text{(A.8d, e, f)}$$

$$Nx_{12} + Nz_{23} \cdot \tan v = 0, \qquad Ny_{12} - Nz_{23} \cdot \frac{\tan\mu - \tan v\cos\alpha}{\sin\alpha} = 0, \qquad Nz_{12} - Nz_{23} = 0, \qquad \text{(A.8g, h, i)}$$

$$Mx_{12} + Nz_{23} \cdot \frac{\tan\mu}{\sin\alpha} \cdot l = 0, \qquad My_{12} = 0, \qquad Mz_{12} + Nz_{23} \cdot \frac{\tan\mu\tan v}{\sin\alpha} \cdot l = 0, \qquad \text{(A.8j, k, l)}$$

$$Nx_{23} - Nz_{23} \cdot \tan\mu = 0, \qquad Ny_{23} - Nz_{23} \cdot \frac{-\tan v + \tan\mu\cos\alpha}{\sin\alpha} = 0, \qquad Nz_{23} - Nz_{23} = 0, \qquad \text{(A.8m, n, o)}$$

$$Mx_{23} + Nz_{23} \cdot \frac{\tan v}{\sin\alpha} \cdot l = 0, \qquad My_{23} = 0, \qquad Mz_{23} - Nz_{23} \cdot \frac{\tan\mu\tan v}{\sin\alpha} \cdot l = 0, \qquad \text{(A.8p, q, r)}$$

$$Nx_{32} + Nz_{23} \cdot \tan v = 0, \qquad Ny_{32} - Nz_{23} \cdot \frac{-\tan\mu + \tan v\cos\alpha}{\sin\alpha} = 0, \qquad Nz_{32} + Nz_{23} = 0, \qquad \text{(A.8s, t, u)}$$

$$Mx_{32} - Nz_{23} \cdot \frac{\tan\mu}{\sin\alpha} \cdot l = 0, \qquad My_{32} = 0, \qquad Mz_{32} + Nz_{23} \cdot \frac{\tan\mu\tan v}{\sin\alpha} \cdot l = 0. \qquad \text{(A.8v, w, x)}$$

The 24×24 coefficient matrix of the set of homogeneous linear equations (A.8) is the *equilibrium matrix*. Taking (8), (A.4) and (A.6) into account, symbolic calculation yields that, for $0° \leqslant \alpha \leqslant 180°$, $-180° < \theta < 180°$ and $-180° < \varphi < 180°$, the rank deficiency of the equilibrium matrix is 1. This changes at $\alpha = 90° \pm 30°$, $\theta = \varphi = \pm 180°$, where the rank deficiency of the equilibrium matrix becomes 2.

References

Baker, J.E., 1980. An analysis of Bricard linkages. Mechanism and Machine Theory 15, 267–286.

Ball, W.W.R., Coxeter, H.S.M., 1987. Mathematical Recreation & Essays, thirteenth ed. Dover, New York, pp. 154–155.

Bennett, G.T., 1905. The parallel motion of Sarrus and some allied mechanisms. Philosophical Magazine, 6th Series 9, 803–810.

Bennett, G.T., 1911. Deformable octahedra. Proceedings of the London Mathematics Society, 2nd Series 10 (1), 309–343.

Bricard, R., 1897. Mémoire sur la théorie de l'octaedre articulé. Journal de mathématiques pures et appliquées, Liouville 3, 113–148.

Bricard, R., 1927. Leçons de cinématique, vol. 2. Gauthier-Villars, Paris, pp. 7–12.

Calladine, C.R., 1978. Buckminster Fuller's "tensegrity" structures and Clerk Maxwell's rules for the construction of stiff frames. International Journal of Solids and Structures 14, 161–172.

Calladine, C.R., Pellegrino, S., 1991. First-order infinitesimal mechanisms. International Journal of Solids and Structures 27 (4), 505–515.

Chen, Y., 2003. Design of Structural Mechanisms. D.Phil. Dissertation, University of Oxford.

Denavit, J., Hartenberg, R.S., 1955. A kinematic notation for lower-pair mechanisms based on matrices. Transactions of the ASME, Journal of Applied Mechanics 22 (2), 215–221.

Dietmeier, P., 1995. A new 6R space mechanism. In: Proceedings of Ninth World Congress on the Theory of Machines and Mechanisms, Milano, vol. 1, pp. 52–56.

Gan, W.W., Pellegrino, S., 2003. Closed-loop deployable structures, AIAA 2003-1450. In: Proceeding of the 44th AIAA/ASME/ASCE/AHS/ASC Structures, Structural Dynamics, and Materials Conference, Norfolk, VA, April 7–10, 2003 (CD-ROM).

Goldberg, M., 1943. New five-bar and six-bar linkages in three dimensions. Transactions of the ASME 65, 649–663.

Hunt, K.H., 1978. Kinematic Geometry of Mechanisms. Clarendon Press, Oxford.

Lengyel, A., 2002. Analogy Between Equilibrium of Structures and Compatibility of Mechanisms. D.Phil. Dissertation, University of Oxford.

Lengyel, A., You, Z., 2003. Analogy between bifurcations in stability of structures and kinematics of mechanisms. Mechanics Based Design of Structures and Machines 31 (4), 491–507.

Lengyel, A., You, Z., 2004. Bifurcations of SDOF mechanisms using catastrophe theory. International Journal of Solids and Structures 41, 559–568.

Mavroidis, C., Roth, B., 1995. New and revised overconstrained mechanisms. Transactions of the ASME, Journal of Mechanical Design 117, 75–80.

Pellegrino, S., You, Z., 1993. Foldable ring structures. In: Parke, G.A.R., Howard, C.M. (Eds.), Space Structures 4, Proceedings of the Fourth International Conference on Space Structures, Guildford, Thomas Telford, London, pp. 783–792.

Phillips, J., 1990. Freedom of Machinery, vol. 2. Cambridge University Press, Cambridge.

Sarrus, P.T., 1853. Note sur la transformation des mouvements rectilignes alternatifs, en mouvements circulaires, et reciproquement. Comptes Rendus Hebdomadaires des Séances de l'Académie des Sciences 36, 1036–1038.

Schattschneider, D., Walker, W., 1977. M.C. Escher Kaleidocycles. Ballantin Books, New York.

Schatz, P., 1998. Rhythmusforschung und Technik, 2. Auflage. Verlag Freies Geistesleben, Stuttgart.

Tarnai, T., 1984. Bifurcation of equilibrium and bifurcation of compatibility. In: Abstracts of Lectures. 16th International Congress of Theoretical and Applied Mechanics, Lyngby, Denmark. Lecture 652.

Tarnai, T., 2001. Kinematic bifurcation. In: Pellegrino, S. (Ed.), Deployable Structures, CISM Courses and Lectures No. 412. Springer, Wien, pp. 143–169, Chapter 8.

Waldron, K.J., 1968. Hybrid overconstrained linkages. Journal of Mechanisms 3, 73–78.

Wohlhart, K., 1987. A new 6R space mechanism. In: Proceedings of the Seventh World Congress on the Theory of Machines and Mechanisms, Sevilla, Spain, vol. 1, pp. 193–198.

Wohlhart, K., 1991. Merging two general Goldberg 5R linkages to obtain a new 6R space mechanism. Mechanism and Machine Theory 26 (2), 659–668.

You, Z., Pellegrino, S., 1997. Cable-stiffened pantographic deployable structures. Part 2: mesh reflector. AIAA Journal 35, 1348–1355.

Zahaurek, F., 1999. Der umpstülpbare Würfel nach Paul Schatz. Available from <http://www.fzk.at/>.